Romanian Reports in Physics, Vol. 68, No. 1, P. 294–304, 2016

A STUDY OF THE LASER-PRODUCED ALUMINUM PLASMA BY MEANS OF COMPUTER SIMULATION

C. IORGA, V. STĂNCĂLIE, V. PĂIŞ

National Institute for Laser Plasma and Radiation Physics, Atomistilor 409, P. O. Box MG-36, Magurele-Ilfov, 077125 Romania EU
Email: *iorga.cristian@inflpr.ro*

Received January 15, 2015

Abstract. We investigate the emission spectrum measured from the laser-produced aluminum plasma experiment held at the nhelix-laser test bed facility at GSI by focusing a Nd-glass YAG laser beam of $50J$ pulse energy, $15ns$ full width half maximum duration and $\lambda = 1.064\mu m$ wavelength, with a spot size of $500\mu m$ on a massive aluminum target. The Flexible Atomic Code (FAC) is employed to obtain the atomic data that will be further used in the fully relativistic collisional radiatiative model to create the synthetic spectra necessary for the line identification. In the atomic modelling we considered the following atomic processes: excitation, deexcitation, photoionization, radiative recombination, electron-ionization, spontaneous radiative decay, dielectronic recombination and autoionization. The hot electrons are considered in the non-Maxwellian electron energy distribution function when the population kinetics is modeled. They are responsible for the increased number of autoionizing levels giving rise to transition enhancement, especially for the Li-like satellite emission in our study. More forbidden and intercombination transitions arising from the doubly excited states are identified for plasma diagnostic purpose. In the second part of this paper we simulate the action of a short pulse ($150fs$), high-intensity ($10^{17}W/cm^2$), P polarized laser beam of $\lambda = 400nm$ on a $2\mu m$ solid aluminum target in order to understand the transient plasma effects on the emission spectrum. The plasma hydrodynamics is modelled using the one-dimensional MULTI-fs code and the history recordings of plasma parameters are further used in a time-dependent collisional radiative model based on the atomic data obtained from FAC. The intense line transitions in the X-ray range are investigated and compared with values from literature.

Key words: plasma interaction, collisional-radiative model, atomic and ionic spectroscopy.

1. INTRODUCTION

The light-matter interaction for high contrast and short laser pulses has numerous applications in material science, technology and fundamental physics such as fast ultra-short X-ray pulses generation [1], inertial confinement fusion (ICF) [2], astrophysics etc. and has been intensively studied throughout the last decades [3], [4], [5], [6]. By focusing a strong laser beam on a solid target, an energy transfer will occur, heating the target, creating a near solid density hot plasma plume [7] that will also

interact with the initial pulse. For a certain contrast the prepulse, mostly consisting of ASE (amplified spontaneous emission), may induce the plasma generation from the solid matter if the threshold intensity is exceeded. Our study focuses on the hydrodynamic and kinetic simulation of the high intensity, short pulse laser-produced plasma on aluminum target. We use the one dimensional MULTI-fs [8] code for plasma generation and its time evolution while with the help of the fully relativistic Flexible Atomic Code [9] we further simulate the aluminum plasma kinetics.

In the context of this paper, an important role is played by the average ionization $Z_i(\rho, T_e)$ which determines the electron number density $n_e = Z_i n_i$ from the ion density n_i and thereby plasma frequency and photon propagation inside the target. This important quantity is calculated on the assumption of local thermal equilibrium (LTE) approximation and it is taken from the EOS tables.

The work is structured as follows. Section 2 presents the line identification of the forbidden and intercombination transitions in the emission spectrum of the laser-produced plasma at GSI for diagnostic purposes. The influence of the hot electron percentages is expressed using the two-temperature Maxwellian in the collisional radiative model. Section 3 treats the laser-produced plasma for a high intensity laser beam ($I \approx 10^{17} W/cm^2$) in order to simulate the time dependence of the emission spectrum. Comparisons with experimental and theoretical works are provided whenever possible showing a good agreement between our results. Section 4 gives our conclusion remarks.

2. INTERCOMBINATION AND FORBIDDEN X-RAY TRANSITIONS INVESTIGATION IN ALUMINUM PLASMA

We analyze the emission spectrum of the plasma obtained at the nhelix-laser test bed facility at GSI [10], where a Nd-glass YAG laser with the pulse of $\tau = 15ns$ and wavelength $\lambda = 1.064\mu m$ is focused on a massive aluminum target. The mechanism that enables forbidden transitions to have relatively high intensities is described by depressing the allowed transitions while the forbidden ones are kept opacity free. This is achieved through increasing the values of the line center optical thickness, a physical quantity proportional to the radiative decay, $\tau_{0,ij} \sim A_{ji}$.

Large scale (mm) dense ($n_e \approx 10^{21} cm^{-3}$) plasma is produced in order to investigate the validity of the proposed mechanism. The emission spectrum has been recorded in the range of $0.77nm - 0.84nm$ and it mainly consists of transitions belonging to the He-like and Li-like Al ions. These transitions can be resonances screened by a spectator electron in the $n' = 2$ shell, two-electron transitions (both n and l quantum numbers change simultaneously for two different electrons), intercombination (dipole transitions $n = 2 \rightarrow 1$ while changing the spin $\Delta S = 1$) and high-order intercombination transitions (dipole transitions $n = 2 \rightarrow 1$ while changing

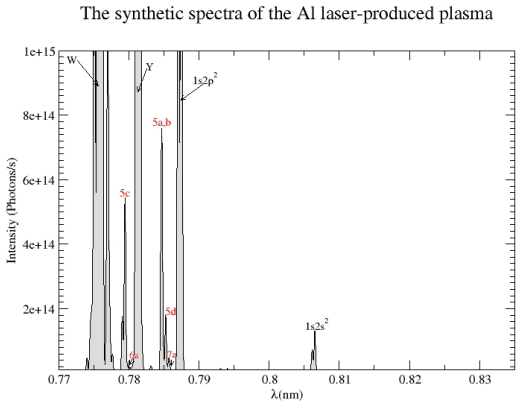

Fig. 1 – The synthetic spectra of the Al plasma emission for the conditions presented in the GSI experiment

the spin of the optical electron with configurations having spectator electrons in shells with $n' > 2$). The calibration is done by using the Al II K_α emission lines caused by the hot electrons from the expanding plasma hitting the solid surface. Intercombination and forbidden transitions from autoionizing states have been identified in this experiment to be used as diagnostic tools in plasma spectroscopy.

We use the collisional radiative model to simulate the emission spectra of the aluminum plasma by taking into account the excitation, deexcitation, photoionization, radiative recombination, radiative decay, electron impact ionization, autoionization and dielectronic recombination processes. In this model we include the electric dipole, magnetic dipole, electric quadrupole and magnetic quadrupole allowed transitions. The atomic data are obtained from the Flexible Atomic Code. A total number of 1500 energy levels have been included in the model to attain the desired accuracy. The plasma parameters necessary to start the collisional radiative model correspond to the experimental conditions mentioned above. The emission spectrum is plotted in Fig.1. Comparing our calculation with those corresponding to the already identified transitions presented in [10], we observe a good agreement between our results in Table 1 and Table 2, with discrepancies less than $30m$Å for wavelengths. It is necessary to stress out the fact that the energy levels obtained with FAC are decently accurate for this type of calculation as can be seen from the data provided earlier in the tables and by comparison with the results from NIST, thus allowing us to further investigate and identify the transition lines emitted from the aluminum plasma.

The He-like resonance, $W = 1s2p(^1P_1) \rightarrow 1s^2(^1S_0) + h\nu$ ($0.775829nm$[1], $0.775860nm$[2]) and intercombination transition $Y = 1s2p(^3P_1) \rightarrow 1s^2(^1S_0) + h\nu$ ($0.780795nm$[1], $0.781303nm$[2]) are easily recognized due to their high line inten-

sity and narrow line width. The values on the left are from this work while those on the right are from NIST. The synthetic spectrum resembles the one measured exper-

Table 1

Observed transitions originating from Li-like Al autoionizing levels $1s2l2l'$

Transition	λ(Å), Decay rate (s^{-1})
2a) $1s(2s2p\ ^3P)\ ^4P_{5/2} - 1s^2 2s\ ^2S_{1/2}$	$7.9400/7.9299/7.9333/7.9412$
	$1.97/-/-/1.91 \times 10^7$
2b) $1s(2s2p\ ^3P)\ ^4P_{3/2} - 1s^2 2s\ ^2S_{1/2}$	$7.9425/7.9323/7.9359/7.9437$
	$1.60/1.57/1.18/1.57 \times 10^{10}$
2c) $1s(2s2p\ ^3P)\ ^4P_{1/2} - 1s^2 2s\ ^2S_{1/2}$	$7.9434/7.9333/7.9374/7.9446$
	$6.17/5.95/4.48/6.06 \times 10^9$
2d) $1s(2s^2\ ^1S)\ ^2S_{1/2} - 1s^2 2p\ ^2P_{1/2}$	$8.0610/8.0764/8.0784/8.0873$
	$5.43/4.17/5.53/4.66 \times 10^{11}$
2e) $1s(2s^2\ ^1S)\ ^2S_{1/2} - 1s^2 2p\ ^2P_{3/2}$	$8.0649/8.0802/8.0821/8.0910$
	$9.78/7.68/1.02/8.57 \times 10^{11}$

imentally. In Table 1 and Table 2 each row corresponds to a certain transition and contains 4 values for wavelength and radiative decay rate given by the present work done with Flexible Atomic Code (1^{st}) and the results from [10] using the MZ method (2^{nd}), the HFR method (3^{rd}), and the MCDF method (4^{th}).

Table 3 contains the transitions belonging to the Li-like ions of the aluminum plasma in the corresponding energy range. By comparing the synthetic spectra with the one measured at GSI we have observed 4 inner-shell-excited satellite transitions (group "5a-5d") and two high-order intercombination transitions ("6a,7a") with relatively high line intensity. Data from NIST are provided when possible for comparison purpose.

The level configurations $^4P_{5/2}$,$^4P_{3/2}$ radiatively decay to the ground state of the Li-like Al ion through magnetic quadrupole transition with small decay rates $1.97 \times 10^7/3.18 \times 10^6 s^{-1}$, while $^4P_{3/2}$,$^4P_{1/2}$ decay to the ground state *via* electric dipole transition with $1.60 \times 10^{10}/6.17 \times 10^9 s^{-1}$ rates. The $1s(2s^2\ ^1S)\ ^2S_{1/2}$ level configuration decays to $1s^2 2p\ ^2P_{1/2}$ *via* electric dipole ($5.43 \times 10^{11} s^{-1}$) or to $1s^2 2p\ ^2P_{3/2}$ via electric dipole ($9.78 \times 10^{11} s^{-1}$) and magnetic quadrupole ($1.69 \times 10^6 s^{-1}$) allowed transitions. The electric dipole allowed "5a,b" lines have the highest radiative decay rates with at least three orders of magnitude higher than all other transitions with the same upper level. The same applies for the "5c,d" transitions independent on the lower level configuration splitting. Despite its low intensity, the high-order intercombination transition "6a" is observed in the spectrum due to the lack of emission lines with photon energies in this range. Different transitions having the

Table 2

Observed high-order doublet intercombination transitions originating from Li-like Al autoionizing levels $1s2l3l'$

Transition	λ(Å), Decay rate (s^{-1})
(3a)$(1s2p\ ^3P)3d\ ^2D_{5/2} - 1s^2 3d\ ^2D_{3/2}$	$7.8212/7.8245/7.8304/7.8332$ $1.12/2.43/1.48/1.31 \times 10^{11}$
(3a)$(1s2p\ ^3P)3d\ ^2D_{3/2} - 1s^2 3d\ ^2D_{3/2}$	$7.8215/7.8247/7.8308/7.8335$ $2.58/2.25/3.14/3.01 \times 10^{11}$
(3a)$(1s2p\ ^3P)3d\ ^2D_{5/2} - 1s^2 3d\ ^2D_{5/2}$	$7.8216/7.8248/7.8307/7.8335$ $3.94/1.80/3.06/2.96 \times 10^{11}$
(3b)$(1s2p\ ^3P)3p\ ^2P_{1/2} - 1s^2 3p\ ^2P_{1/2}$	$7.8548/7.8349/7.8403/7.8437$ $29.11/11.2/10.9/8.96 \times 10^{11}$
(3b)$(1s2p\ ^3P)3p\ ^2P_{3/2} - 1s^2 3p\ ^2P_{1/2}$	$7.8542/7.8349/7.8402/7.8436$ $6.39/4.92/4.32/3.42 \times 10^{11}$
(3b)$(1s2p\ ^3P)3p\ ^2P_{1/2} - 1s^2 3p\ ^2P_{3/2}$	$7.8553/7.8359/7.8414/7.8447$ $4.69/3.65/3.94/2.87 \times 10^{11}$
(3b)$(1s2p\ ^3P)3p\ ^2P_{3/2} - 1s^2 3p\ ^2P_{3/2}$	$7.8558/7.8360/7.8412/7.8446$ $26.1/13.3/13.7/11.2 \times 10^{11}$

same upper level emerge with even higher radiative decay rate, such as the allowed electric dipole $1s^2 2p(^2P^o_{3/2}) - 1s^2 3s(^2S_{1/2})$ transition with $A = 1.85 \times 10^{12} s^{-1}$, although it is difficult to observe them due to the fact that they are strongly blended in the spectrum. We also mention that an electric quadrupole allowed transition $1s2p(^3P^o_2)\ 3d(^2P^o_{3/2}) - 1s^2 2p(^2P_{3/2})$ reaches the value of $A = 1.07 \times 10^9 s^{-1}$, which is relatively high in this energy range. The $1s[2s3s(^1S_0)](^2S_{1/2})$ level can decay via electric dipole transitions on $1s^2 2p(^2P_{1/2})$ $(A = 1.61 \times 10^{11} s^{-1})$, $1s^2 2p(^2P_{3/2})$ $(A = 1.49 \times 10^{11} s^{-1})$, $1s^2 3p(^2P_{1/2})$ $(A = 1.17 \times 10^{12} s^{-1})$, $1s^2 3p(^2P_{3/2})$ $(A = 1.93 \times 10^{12}\ s^{-1})$, electric quadrupole transitions on $1s^2 3d(^2D_{3/2})$ $(A = 1.05 \times 10^7\ s^{-1})$, $1s^2 3d\ (^2D_{5/2})$ $(A = 1.53 \times 10^7 s^{-1})$, magnetic dipole transition on $1s^2 3d\ (^2D_{3/2})$ $(A = 1.07 \times 10^2 s^{-1})$ and magnetic quadrupole transitions on $1s^2 2p(^2P_{3/2})$ $(A = 2.66 \times 10^5 s^{-1})$, $1s^2 3p(^2P_{3/2})$ $(A = 3.65 \times 10^4 s^{-1})$. By considering the radiative decay rates from above we can approximate the lifetime of $1s[2s3s(^1S_0)]^2S_{1/2}$ to be $2.93 \times 10^{-13} s$. This level is mainly populated through the dielectronic capture process, $1s^2(^1S_0) + e^- \rightarrow 1s(^2S_{1/2})[2s3s(^1S_0)](^2S_{1/2})$, having a relatively high dielectronic capture strength $0.164eV\ Mb$ and sufficient plasma electrons with energy above the threshold. By using the same considerations we compute the lifetime of the other two configurations corresponding to the same level and observe they are more stable, especially the $^4S_{3/2}$ configuration, $1s[2s3s(^3S_1)](^4S_{3/2}) \rightarrow 9.61ns$,

Table 3

Identified high line intensity inner-shell-excited satellite transitions ("5a-5d") compared to NIST values (right) and two high-order intercombination transitions ("6a,7a")

Transition	λ(Å), Decay rate (s^{-1})
5a)$1s[2s2p(^3P^o)](^2P^o_{1/2}) - 1s^2(^1S_0)2s(^2S_{1/2})$	$7.8470/7.8471$
	2.61×10^{13}
5b)$1s[2s2p(^3P^o)](^2P^o_{3/2}) - 1s^2(^1S_0)2s(^2S_{1/2})$	$7.8456/7.8471$
	2.72×10^{13}
5c)$1s[2p^2(^1S_0)](^2S_{1/2}) - 1s^2 2p(^2P^o_{3/2})$	$7.7941/7.7963$
	8.91×10^{12}
5d)$1s[2p^2(^1D_2)](^2D_{3/2}) - 1s^2 2p(^2P^o_{3/2})$	$7.8522/7.8756$
	3.61×10^{13}
6a)$1s2p(^3P^o_2)3d(^2P^o_{3/2}) - 1s^2 3d(^2D_{5/2})$	7.7947
	1.42×10^{12}
7a)$1s[2s3s(^1S_0)](^2S_{1/2}) - 1s^2 3p(^2P^o_{3/2})$	7.8575
	1.93×10^{12}

$1s[2s3s(^3S_1)]\ (^2S_{1/2}) \rightarrow 1.72ps.$

3. TIME EVOLUTION SIMULATION OF THE TRANSIENT PLASMA EMISSION SPECTRA IN FS REGIME FOR THE FOLLOWING LASER PARAMETERS

$\lambda = 400nm,\ I = 10^{17}W/cm^2,\ \tau_{FWHM} = 150fs,\ P\ polarization$

A frequency doubled Ti: sapphire laser, with $\lambda = 400nm$, of peak intensity $10^{16} - 10^{17}W/cm^2$ is used to simulate the ablation process on a $2\mu m$ thick solid aluminum target. The pulses used in this simulation are P-polarized with $\tau_{FWHM} = 150fs$ and have the following form factor:

$$P(t) = P_{max} sin^2(\frac{\pi}{2}\frac{t}{\tau}), \quad 0 \leq t \leq 2\tau \tag{1}$$

The system is initially at room temperature, $T_e = T_i = 0.0258eV$, and density specific to solid aluminum, $\rho = 2.7g/cm^3$. The target is divided into 30 Lagrangian layers, noting that the first nominal layer was set to a significantly smaller thickness having the value of $0.075nm$ to treat the high temperature and density gradients accurately. Another important aspect is the fact that the frequency doubling of incident pulse laser, assumed in our theoretical study, mitigates the severity of the prepulse effect but does not eliminate it. To check the validity of our model calculation results we assumed the effect of a finite $1:10^5$ contrast as in experiments performed by P. Audebert *et al.* [11]. MULTI-fs code is well suited for this purpose and was used

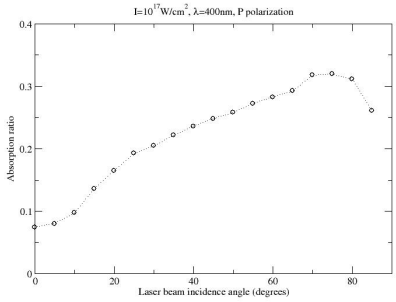

Fig. 2 – The absorption ratio of the laser energy in the target for different angles at constant $I = 10^{17} W/cm^2$, $\lambda = 400nm$, $\tau_{FWHM} = 150fs$, P polarization

previously in literature to model the prepulse effect [12], [13]. In these experiments the prepulse duration is around $500ps$ and may be extended to a few ns.

For high intensities, such as $10^{17} W/cm^2$, the laser beam corresponds to a strong energy absorption in the expanding plasma. Consequently the temperatures are varying from a few eV up to several keV, while the plasma remains at near solid density. By focusing a P-polarized laser pulse at 38^0 incident angle on the target surface, a small component of hot electrons is generated affecting the plasma ionization and transitions line intensity. Depending on the incident angles the absorption mechanisms may alternate.

The absorption ratio for different incident angles at $10^{17} W/cm^2$ laser beam intensity and $\tau_{FWHM} = 150fs$ pulse duration is shown in Fig.2. In close agreement to the experiments in [14] and [15], the maximum absorption takes place at 75^o incidence angle. The maximum value for the absorption ratio is 31.97%, as expected from [16] and [17] given the range of the $I\lambda^2$ parameter. In this femtosecond regime the front layer reaches velocities up to $10^8 cm/s$. The laser deposition in the target at the maximum laser pulse intensity reaches the value of $6.98 \times 10^{28} erg/(gs)$ corresponding to the layer with the temperature of $951.92eV$ and mass density of $0.4226 g/cm^3$. The laser deposition, electron temperature and the mass density are plotted against the target depth in Fig.3 as output from the simulation. To simulate the ionization dynamics of Aluminum we compute the ion fractions in the plasma and plot them in Fig.4.

To include the hot electron component in the model a non-Maxwellian distribution function is employed as follows:

$$f(\epsilon) = (1 - \alpha_H) f_M(T_1) + \alpha_H f_H(\epsilon) \tag{2}$$

where α_H refers to the hot electron component percentage and $f_H(\epsilon)$ is their distribution function component.

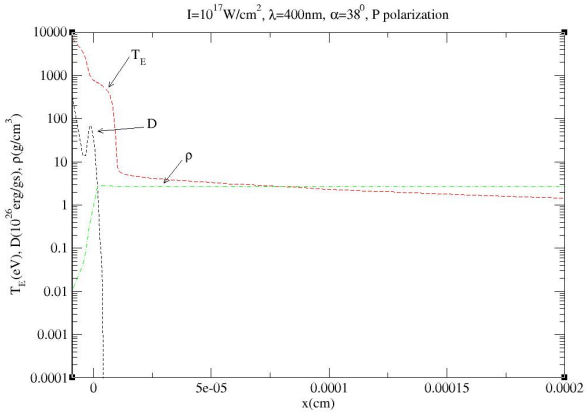

Fig. 3 – The spatial dependence of the laser deposition, electron temperature and mass density at $150fs$ for $I = 10^{17}W/cm^2$, $\lambda = 400nm$, $\tau_{FWHM} = 150fs$, $\alpha = 38^0$, P polarization

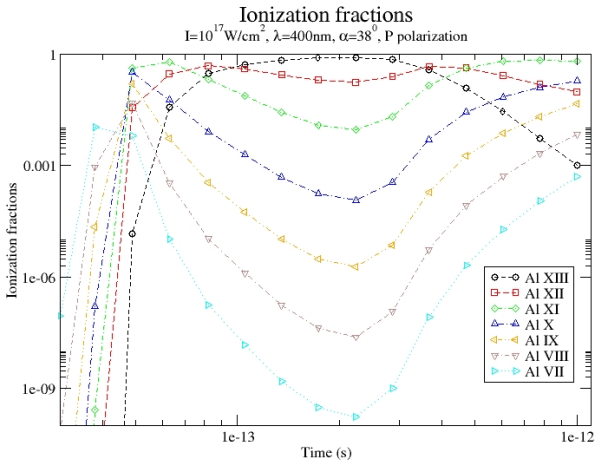

Fig. 4 – The time-dependence of the ionization fractions of the $Al^{6+} - Al^{12+}$ ions in the aluminum plasma

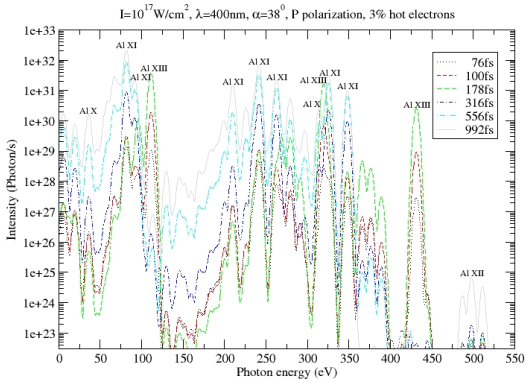

Fig. 5 – The emission spectra of the aluminum plasma for 6 different time steps in the hydrodynamic simulation with a 3% hot electron component of $T_H = 10keV$

In our work we account for a 3% hot electron component having a temperature of $10keV$, value inspired by the theoretical and experimental data reported in [18], [19], [20], [21], [22], [23]. The emission spectrum of the plasma is plotted at 6 different time steps, in the energy range up to $550eV$, $76fs$, $100fs$, $178fs$, $316fs$, $556fs$ and $992fs$ in Fig.5 showing enhancement for transitions belonging to the Al^{9+}, Al^{10+}, Al^{11+} and Al^{12+} ions.

In the spectrum plotted at $76fs$ the enhancement becomes visible at the following wavelengths: $4.250nm, 4,248nm$ and $4.175nm$ corresponding to $1s_{1/2}3p_{1/2}$ $(^3P_1^o)$ $-1s_{1/2}2s_{1/2}(^3S_1)$, $1s_{1/2}3p_{1/2}(^3P_2^o)$ $-1s_{1/2}2s_{1/2}(^3S_1)$ and $1s^22s_{1/2}4d_{5/2}$ $(^3D_3) - 1s^22s_{1/2}2p_{3/2}(^3P_2^o)$ transitions belonging to Al^{11+} and Al^{9+}, respectively. Their line intensity is changed from $1.06 \times 10^{25} Photons/s$ to $3.54 \times 10^{25} Photons$ $/s$, $1.66 \times 10^{25} Photons/s$ to $5.87 \times 10^{25} Photons/s$ and $1.08 \times 10^{25} Photons/s$ to $4.61 \times 10^{25} Photons/s$, respectively. Comparison with theoretical calculations and experimental data from [24], [25] and [26] has showed a good agreement. The corresponding measured wavelengths are $4.258nm$, $4.261nm$ and $4.490nm$ [25].

The emission spectrum plotted for the $992fs$ time step shows several transitions in the soft X-ray range with high line intensity. They are the $1s^23d(^2D)3/2) - 1s^22p(^2P_{1/2}^o)$, $1s^23d(^2D_{5/2}) - 1s^22p(^2P_{3/2}^o)$, and the $1s^23p(^2P_{3/2}^o) - 1s^22s(^2S_{1/2})$ transitions at $5.117nm$, $5.131nm$ and $4.711nm$ wavelengths, respectively each of them with the intensity of $2.73 \times 10^{31} Photons/s$, $4.95 \times 10^{31} Photons/s$ and $1.91 \times 10^{31} Photons/s$. The corresponding measured wavelength values, reported in [25], are $5.229nm$, $5.245nm$ and $4.829nm$.

4. CONCLUSION

A full relativistic collisional radiative calculation has been implemented for the plasma parameters measured from the GSI experiment to verify the validity of the atomic data obtained from Flexible Atomic Code in the case of intercombination and forbidden transitions. The emitted X-rays predicted by our simulation model are in close agreement with those presented in the experiment and other theoretical computations and also those from NIST. Further transition identification has been done for the use in plasma diagnostics. The effects of hot electrons have been included in our model by using a two-temperature Maxwellian component for the electron energy distribution function. The result was that they influence the population kinetics especially enhancing the population of autoionizing states.

In the second part of the paper we simulate the subpicosecond time-variation of the emission spectrum for the $2\mu m$ thick aluminum laser-produced plasma for the following laser parameters: $\lambda = 400nm, I = 10^{17}W/cm^2, \tau_{FWHM} = 150fs, P$ polarization. The Multi-fs code simulates the plasma hydrodynamics in order to provide the plasma parameters necessary for the fully relativistic time-dependent colissional radiative model.

Intense transitions in the X-ray spectrum with wavelengths comparable to other theoretical and experimental work have been identified. Additional enhancement for line intensities has been put into evidence in the Al^{9+} and Al^{11+} spectrum. Therefore a few percentages of hot electrons can significantly alter the ionization dynamics and spectral characteristics of the laser-produced aluminum plasma.

Acknowledgements. This work is partially supported by the Institute of Atomic Physics under project no. F03. Financial support under the Romanian Space Agency coordinated program STAR Project Number 33 is also acknowledged.

REFERENCES

1. J. C. Kieffer, Z. Jiang, A. Ikhlef, C. Y. Cote, O. Peyrusse, Journal of the Optical Society of America B-Optical Physics **13**, 132–137 (1996).
2. J. D. Lindl, P. Amendt, R. L. Berger, S. G. Glendinning, S. H. Glenzer, S. W. Haan, R. L. Kauffman, O. L. Landen, L. J. Suter, Physics of Plasmas **11**, 339–491 (2004).
3. R. Fedosevs, R. Ottman, R. Siegel, G. Kuhnle, Phys Rev Lett **64**, 1250–1253 (1990).
4. U. Teubner, J. Bergmann, B. Van Wonterghem, F. P. Schafer, R. Sauerbrey, Phys. Rev. Lett. **70**, 794–797 (1993).
5. J. C. Gauthier, J. P. Geindre, P. Audebert, D. Bastiani, C. Quoix, G. Grillon, A. Mysyrowicz, A. Antonetti, R. C. Mancini, Physics of Plasmas **4**, 1811 (1997).
6. J. Osterholz, F. Brandl, M. Cherchez, T. Fischer, D. Hemmers, B. Hidding, A. Pipahl, G. Pretzler, S. J. Rose, O. Willi, Physics of Plasmas **15**, 103301 (2008).
7. K. Eidmann, J. Meyer-Ter-Vehn, T. Schelegel, S. Huller, Phys Rev Lett **64**, 1202–1214 (2000).
8. R. Ramis, K. Eidmann, J. Meyer-Ter-Vehn, S. Huller, Computer Physics Communications **183**,

637–655 (2012).
9. M. F. Gu, Can. J. Phys. **86(5)**, 675–689 (2008).
10. F. B. Rosmej, D. H. Hoffmann, W. Süß, M. Geißel, Y. Faenov, A, T. A. Pikuz, Physical Review A **63**, 032716 (2001).
11. P. Audebert, R. Shepher, K. B. Fournier, O. Peyrusse, D. Price, R. Lee, P. Springer, J.-C. Gauthier, L. Klein, Phys. Rev. Lett. **89**, 265001 (2002).
12. M. Kaluza, J. Schreiber, J. J. Honrubia, M. I. K. Santala, G. D. Tsakiris, K. Eidmann, J. Meyer-ter Vehn, K. J. Witte, Phys. Rev. Lett. **93 No. 4**, 045003 (2004).
13. K. J. Witte, U. Andiel, K. Eidmann, E. Fill, C. Gahn, *et al.*, in *IAEA-IFP/08* (2001).
14. M. Cherchez, R. Jung, J. Osterholz, T. Toncian, O. Willi, Phys. Rev. Lett. **100**, 245001 (2008).
15. D. F. Price, R. M. More, G. Walling, R S Guethlein, R. L. Shepher, R. E. Stewart, W. E. White, Phys. Rev. Lett. **75**, 252–255 (1995).
16. J. R. Davies, in *Plasma Phys. Control. Fusion 51*, p. 014006 (2009).
17. E. M. Campbell, Phys. Fluids B **4**, 3781–3799 (1992).
18. H. Chen, R. Stepherd, H. K. Chung, A. Kemp, S. B. Hansen, *et al.*, Physical Review E **76**, 056402 (2007).
19. A. Moinard, F. Petitdemange, J. Larou, F. B. Rosmej, in *EPJ Web of Conferences 59,13003* (2013).
20. G. Malka, J. L. Miquel, Physical Review Letters **77**, 75–78 (1996).
21. J. Psikal, V. Tikhonchuk, J. Limpouch, O. Klimo, Journal of Physics: Conference Series **244** (2010).
22. S. Weber, G. Bonnaud, J.-C. Gauthier, Physics of Plasmas **8**, 387 (2001).
23. Y. Sentoku, K. Mima, T. Taguchi, S. Miyamoto, Y. Kishimoto, Physics of Plasmas **5**, 4366 (1998).
24. J. A. Fernley, K. T. Taylor, M. J. Seaton, J. Phys. B: At. Mol. Phys. **20**, 6457–6476 (1987).
25. E. Ferner, Ark. Mat. Astron. Fys. **36A(a)**, 1–65 (1948).
26. J. A. Tully, M. J. Seaton, K. A. Berrington, J. Phys. B: At. Mol. Phys. **23**, 3811–3837 (1990).